*Article*

# Biomechanical Analysis of Staples for Epiphysiodesis

Karel Frydrýšek [1,2,*], Daniel Čepica [1,2], Tomáš Halo [1,2], Ondřej Skoupý [1,2], Leopold Pleva [1,3], Roman Madeja [1,3], Jana Pometlová [1,3], Monika Losertová [4,5], Jan Koutecký [5], Pavel Michal [5], Vojtěch Havlas [6], Šimon Kraus [6,7], Dominik Ďurica [7], Kateřina Peterek Dědková [8], Marek Pagáč [9], Pavel Krpec [10] and Paweł Osemlak [11]

1   Institute of Emergency Medicine, Faculty of Medicine, University of Ostrava, Syllabova 19, 703 00 Ostrava-Vítkovice, Czech Republic; daniel.cepica@vsb.cz (D.Č.); tomas.halo@vsb.cz (T.H.); ondrej.skoupy@vsb.cz (O.S.); leopold.pleva@fno.cz (L.P.); roman.madeja@fno.cz (R.M.); jana.pometlova@fno.cz (J.P.)
2   Department of Applied Mechanics, Faculty of Mechanical Engineering, VSB—Technical University of Ostrava, 17. Listopadu 2172/15, 708 00 Ostrava, Czech Republic
3   Trauma Center, 17., University Hospital Ostrava, Listopadu 1790, 708 52 Ostrava-Poruba, Czech Republic
4   Faculty of Materials Science and Technology, VSB—Technical University of Ostrava, 17. Listopadu 2172/15, 708 00 Ostrava, Czech Republic; mlosertova@vsb.cz
5   Medin, a.s, Vlachovicka 619, 592 31 Nové Město na Moravě, Czech Republic; jan.koutecky@medin.cz (J.K.); pavel.michal@medin.cz (P.M.)
6   Motol University Hospital, V Úvalu 84, 150 06 Prague 5, Czech Republic; vojtech.havlas@lfmotol.cuni.cz (V.H.); simon.kraus@seznam.cz (Š.K.)
7   Department of Orthopaedics, Second Faculty of Medicine, Charles University, V Úvalu 84, 150 06 Prague 5, Czech Republic; dom.durica@gmail.com
8   Center of Advanced Innovation Technologies, VSB—Technical University of Ostrava, 17. Listopadu 15/2172, 708 00 Ostrava-Poruba, Czech Republic; katerina.peterek.dedkova@vsb.cz
9   Department of Machining, Faculty of Mechanical Engineering, VSB—Technical University of Ostrava, Assembly and Engineering Metrology, 17. Listopadu 2172/15, 708 00 Ostrava, Czech Republic; marek.pagac@vsb.cz
10  V-NASS, a.s., Halasova 2938/1a, 703 00 Ostrava-Vítkovice, Czech Republic; pavel.krpec@v-nass.cz
11  Pediatric University Hospital Named by Prof. Antoni Gębala in Lublin, ul. Prof. A. Gębali 6, Department of Pediatric Surgery and Traumatology, Medical University of Lublin, 20-093 Lublin, Poland; posem1@poczta.onet.pl
*   Correspondence: karel.frydrysek@vsb.cz; Tel.: +420-597323495; Fax: +420-596916490

**Abstract:** Limb asymmetry can, and often does, cause various health problems. Blount bone staples (clips) are used to correct such uneven growth. This article analyzes the performance of a biomechanical staple during bone (tibia) growth arrest. The staples considered in this study were made of 1.4441 stainless steel, the model of tibia consisted of two materials representing *corticalis* and *spongiosis*. Hooke's law was used for modeling materials' behaviors for finite element analysis (FEA). The maxima of stress and total staple displacement were evaluated using the finite element method and verification of the results, along with the determination of the maximum loading (growing) force that the staples are capable of withstanding, was performed experimentally. The presented method can be used to determine the safety and usability of staples for bone growth arrest. According to our results, the design of Blount staples considered in this paper is safe and suitable for orthopedic treatment.

**Keywords:** biomechanics; orthopedics; Blount staple; FEA; experiment; epiphysiodesis
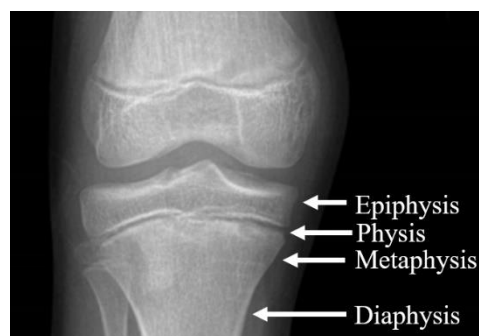
## 1. Introduction

The growth deformities, one of which is Blount's disease, are globally among the most common conditions to present in pediatric orthopedic clinics [1,2]. These deformities can, although rarely, be associated also with childhood obesity, i.e., high body mass index (BMI); for further information, see [3].

These growth deformities have been, for many years, treated surgically, utilizing the manipulation of natural growth capabilities of the bone; see [1]. Epiphyseal stapling is one of the most commonly and traditionally used methods for such correction, using inert metal staples (clips) implanted into a specific part of a child's long bone to temporarily prevent its growth. Hence, epiphyseal stapling (also known as epiphysiodesis, Blount epiphysiodesis, bone growth restriction, or bone growth surgery) involves placing such staples in a way to bridge the growth plate to slow down the growth of the long bone; see [1,4]. This short surgical procedure is performed under general anesthesia.

There are no comparable nonsurgical alternatives to epiphyseal stapling. Surgical alternatives include leg shortening (i.e., a surgery during which a section of the bone is cut out and fragments are joined together with a plate), percutaneous epiphysiodesis, see [5], open epiphysiodesis, and, recently, tension band technique.

Epiphyseal stapling was introduced by Walter Blount in 1949, see [6], and since then, it has become a common procedure of correcting, in particular, angular deformities of the knee (*genu varum* or *genu valgum*) in children. The growth of the child's or adolescent's bone is associated mainly with physis, i.e., a cartilage structure near joints; see [1,4]. Blount staples are also used for pseudoarthrosis treatment [7].

Using staples, the physis (epiphyseal plate) can be relatively simply restrained either on both sides when correcting limb length discrepancy (i.e., "epiphysiodesis") or only on one side when correcting angular deformities (i.e., "hemiepiphyseodesis") (see Figures 1 and 2). Unlike the irreversible method of permanent epiphysiodesis, see [8], epiphyseal stapling does not destroy the epiphyseal plate and, therefore, allows resumption of the growth once the optimal correction is achieved; see [4].



**Figure 1.** Parts of the growing bone (tibia).

Recently, the tension band technique, introduced by Stevens in 2007 [9], using non-locking plates (similar to those used for osteosynthesis) and screws almost in the same position as staples, has gradually become a preferable alternative to stapling. However, Blount's original method still remains an effective means for the treatment of lower limb deformities in adolescents; see [1,4,10].

According to [1,4], besides accurate diagnosis confirmed by a radiogram of the whole limb (see Figure 2), good timing of the treatment is also very important. The surgical procedure involves a short longitudinal incision through soft tissues over the physis and extraperiosteal implantation of the staple using a special instrument under radiography control [11] (see Figure 3). The staple must bridge the physis but not penetrate it to prevent its impairment (see Figure 4).

The staples should not be restricting the physis for longer than 2 years to prevent permanent growth cessation [12]. Other complications during treatment, such as damaging the physis by imprecise staple implantation, mechanical failure of the staple (bending, rarely break), or staple migration can occur. The last one is also the most common complication and disadvantage compared with the tension band technique; see [1,4].
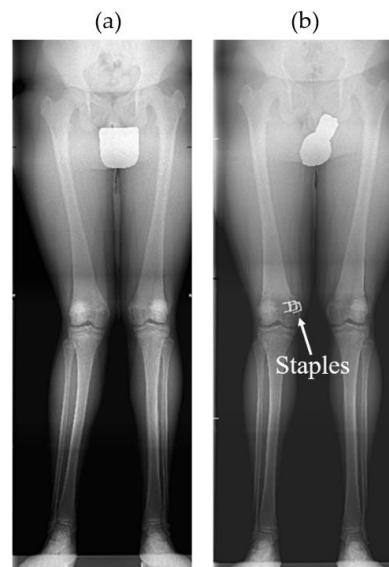
**Figure 2.** (**a**) Long radiogram of preoperative *genu valgum* and (**b**) consecutive correction with staples in femur; see [4].



**Figure 3.** Implantation of staples.



**Figure 4.** Position of staples bridging the physis in femur.

There is a lack of information regarding the biomechanical aspect of Blount's staples; hence, one of the goals of our publishing is to fill the gap in this field.

There are two main methods for solving biomechanical problems:

- Numerical approach—(the main subject of this paper).
- Experimental approach (used and described only marginally here).

In this paper, the stress and deformation of staples during epiphysiodesis are evaluated by a numerical approach using finite element analysis (FEA). The finite element method (FEM) is a recognized instrument of numerical analysis widely used in engineer-

ing mechanics (see, e.g., [13]) and biomechanics. It has been previously used for various biomechanical tasks [14–16], including Blount staple applications in epiphysiodesis [17].

To verify the results of the numerical solution, i.e., to assess the usability of staples under the chosen loading (growing) force, and to find the maximum loading (growing) force that the staples can withstand, a simple experimental approach was also used in this paper. Experiments can be used in combination with FEA (as we do here or, e.g., in [18]), or experiments can serve as a standalone tool for simulation of reality, see, e.g., [19].

Our approach can be further used for another types or modifications of Blount's staples, plates, and similar implantates.

## 2. Materials and Methods

The bone growth occurs in the epiphyseal plate, where a new bone mass is created. Considering this fact, the simulation of the growing process turned out to be difficult. For this reason, we came up with a solution where the artificial bone (tibia) is cut in two at the position of the epiphyseal plate; furthermore, we assume that the bone grows predominantly in the direction of the bone axis (i.e., only oppositional growth is considered), which means that growth can be simulated by pulling the two bone segments away from each other.

Models of the staples, both 3D CAD and physical, were provided by MEDIN, a.s.; see Figure 5 and [20].
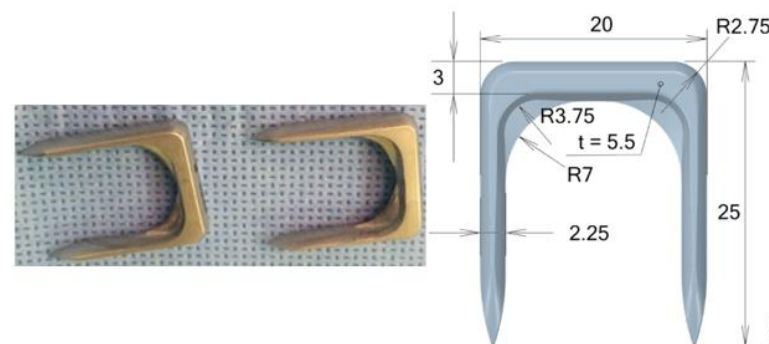


**Figure 5.** Physical model and 3D CAD model with main dimensions (mm), supplied by MEDIN, a.s.

### 2.1. Finite Element Analysis

The numerical analysis is performed using the Ansys Workbench 2020 R2 sw; see [21]. Homogenous and isotropic material models are assumed to be good approximations of reality. Staples are made of biocompatible stainless steel 1.4441 (AISI 316L), see [4], and the artificial bone model consists of *corticalis* and *spongiosis* (i.e., the cortical and spongy parts); mechanical properties were taken from [22], where Young's modulus for *spongiosis* was reported to range between 0.1 and 0.5 GPa and for *corticalis* between 12 and 18 GPa. From this, values closer to the upper limit were chosen; this can, for example, illustrate obesity (i.e., stronger bones to accommodate for higher body mass). Used material models are presented in Table 1.

**Table 1.** Material models of bone and stainless steel.

| Material | Young's Modulus (GPa) | Poisson's Ratio (1) | Yield Strength (MPa) | Ultimate Strength (MPa) |
|---|---|---|---|---|
| 1.4441 | 183 | 0.33 | 690 | 800 |
| *Corticalis* | 16.1 | 0.3 | | |
| *Spongiosis* | 0.4 | 0.3 | | |

Research by Halo et al. [4] focused on a simpler bone material model, considering the cortical part as the only material of the bone. In the current paper, however, we improved the bone material model by dividing it into *corticalis* and *spongiosis* parts.

### 2.1.1. CAD and FEM Model

The used CAD model obtained from a 3D scan and the bone model used in the experiment are not 100% identical; nevertheless, they are sufficiently similar to allow experimental verification of the calculation results; see Figure 6. The model of the whole bone is not necessary for our purposes and, for this reason, only the proximal part of the tibia was used in this calculation. This proximal part was then "cut" in two at the site of the epiphyseal plate. The staples were virtually placed in the bone in the way they usually are during epiphysiodesis, i.e., in the general area bridging the physis.
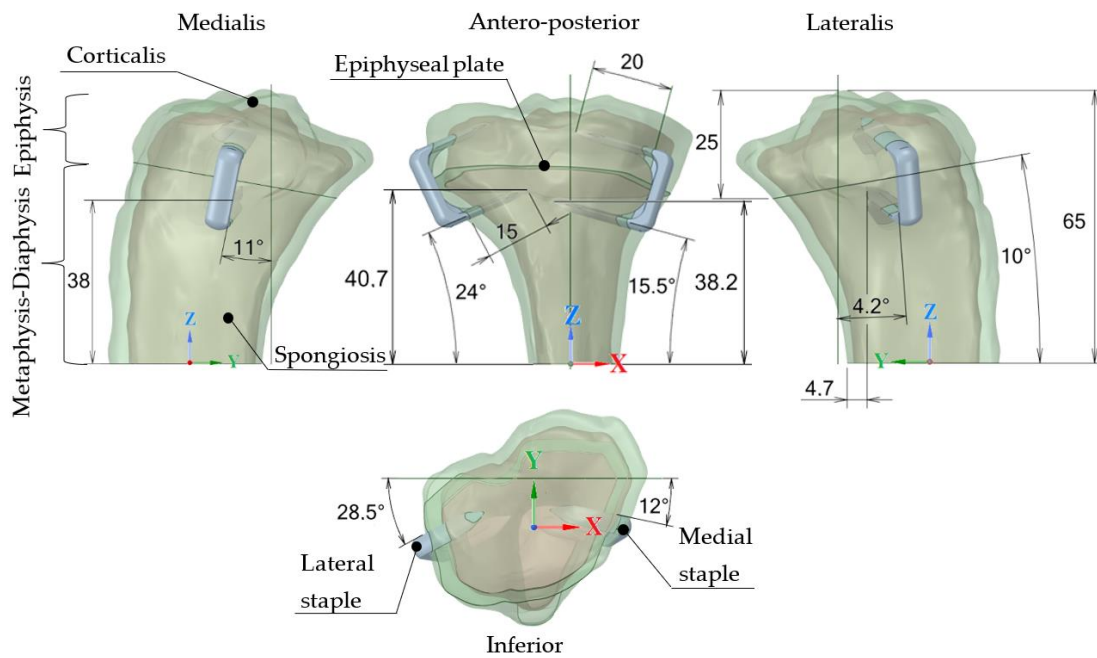


**Figure 6.** 3D CAD model of the bone and staples with main dimensions (mm).

The CAD model of staple provided by MEDIN a.s. contains notches, which are not suitable for FEA. For this reason, sharp edges were rounded; see Figure 7. However, these sharp edges are important for properly inserting the staple in a bone.
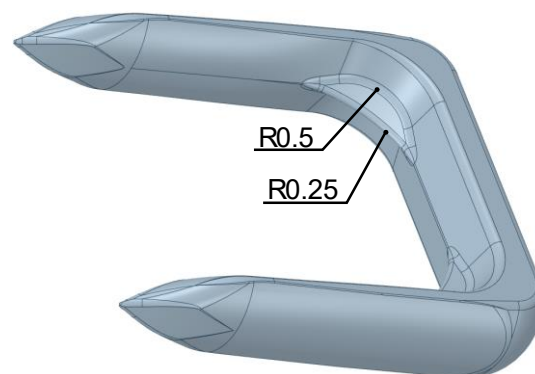


**Figure 7.** 3D CAD model of the staple with rounded sharp edges (mm).

The radius size of 0.25 mm, according to Figure 7, is quite small, because this part of the staple is relatively thin, and using bigger radius size (e.g., 0.5 mm) would result in near complete removal of this part.

In this paper, we used only the bone model and staples for FEA. The reason for this acceptable simplification lies in the fact that the limb growth is primarily determined by the bone (or, more accurately, epiphyseal plate). The bone is intact (i.e., without fracture); therefore, the influence of the muscles, ligaments, menisci, and synovia on bone growth is negligible compared to the load on the bone.

Muscles, ligaments, menisci, and synovia could play a small role in restricting the staple migration, but this effect is not noticeable in our study and hence is considered negligible. Thus, muscle and other tissues and fluids were omitted in this paper.

The influence of anatomical parts in cavitas articularis (i.e., mentioned muscles, ligaments, menisci, and synovia) might play significant role in ambulation of patients with Blount staples, see [23].

The transformation of the CAD model into the FEM model is presented in Figure 8. Considering the complexity of the bone shape, the tibia was discretized by tetrahedral elements (SOLID187 in Ansys sw) with a global maximum size of 2.5 mm. The element size in holes for staples was locally refined to mirror the element size of the staples. In addition, a refinement to 0.5 mm was performed in a small circular area in the immediate vicinity of holes for staples. The global element size is relatively large as we are focusing on and evaluating only the staple response, not that of the bone. The *corticalis* and *spongiosis* FE meshes are continuously connected by nodes and elements sharing faces (i.e., conformal mesh achieved by shared topology function in Ansys SpaceClaim sw), see [21].
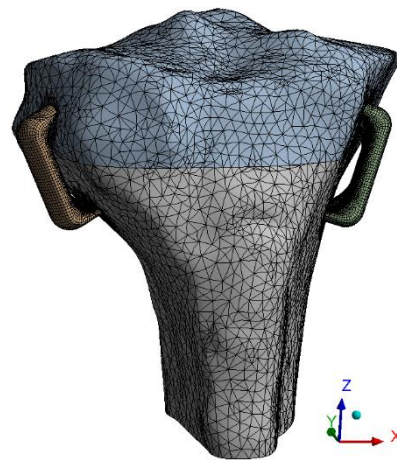


**Figure 8.** FEM model of the bone and staples.

Staples were discretized by a hex-dominant mesh (SOLID186 + some SOLID187 elements) with a global maximum element size of 0.5 mm. The element size was locally refined on radii and in the immediate vicinity of these areas; see Figure 9.

The presented mesh in its final form was used for the final calculation and result evaluation. The sensitivity analysis started with a coarse mesh, and after each computation, a new, refined, mesh with half the element size of the previous mesh was created. This process was repeated until results for two different meshes were close (within a 1% margin of error); in this way, the mesh sensitivity analysis was performed.

Additional information about FE mesh regarding the number of elements and nodes is presented in Table 2.
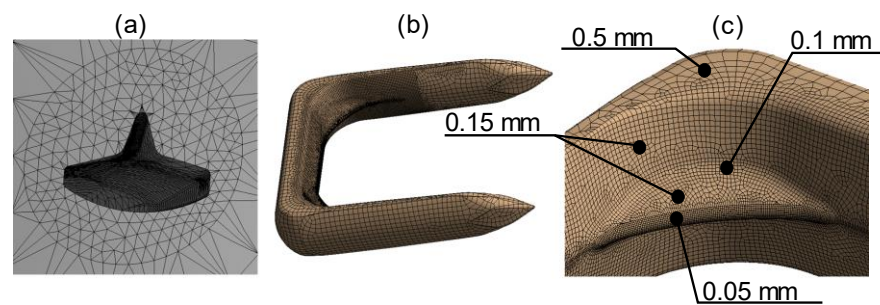
**Figure 9.** Refined FE mesh: (**a**) Detail of the mesh in/around the hole for the staple; (**b**) Mesh of the staple; (**c**) Element size on staple (mm).

**Table 2.** Number of FE elements and nodes.

| Part | | Number of FE Elements | Number of FE Nodes |
|---|---|---|---|
| Tibia | Epiphysis | 66,083 | 102,706 |
| | Metaphysis-Diaphysis | 80,183 | 126,033 |
| Staple | Medial | 132,292 | 438,008 |
| | Lateral | 132,581 | 442,394 |
| Total | | 411,139 | 1,109,141 |

### 2.1.2. Boundary Conditions

The global coordinate system was oriented so that the $Z$-axis is parallel to the bone axis. As mentioned above, we assumed that the bone grows predominantly in the direction of the bone axis (i.e., oppositional growth) and, therefore, the alignment of the axes allows simple loading of the bone segments in the epiphyseal plate in the $Z$ direction. We assumed that for the growth to occur, the loading force Fz needs to match the weight of the person. As the bone growth happens in the early stages of life (childhood, adolescence), we have chosen our bone to come from an adolescent standing on one leg with a chosen 100 kg body weight equivalent to Fz = 980.7 N. In [24], the growing force was determined to be approximately 500 N, i.e., our force Fz was overestimated to err on the side of safety. The force boundary condition is illustrated in Figure 10.

The distal end of the cut tibia is fully fixed (i.e., prescribed displacements are $u_x = u_y = u_z = 0$); in the proximal part; there is a partial fixation (i.e., prescribed displacements $u_x = u_y = 0$) allowing for a movement in the $Z$ direction. Deformation boundary conditions are shown in Figure 11.

Apart from the force and deformation boundary conditions, frictional contacts between the staples and the bone must be considered. The Coulomb friction coefficient between stainless steel and bone ranges from approximately 0.25 to 0.7, according to [25]. The friction coefficient is highly dependent, among other things, on the surface quality of both bone and steel, hardness of bone, etc. In this analysis, the friction coefficient was set to 0.2 (estimated by an educated guess), giving the possibility for staples to migrate out of bone. The friction coefficient used in this study is lower than in [25], taking into account the body fluids and tissues reducing the friction. Nevertheless, even with the low friction coefficient used in our study, the displacement in contact areas was very small, so friction does not have a major effect on stress distribution.
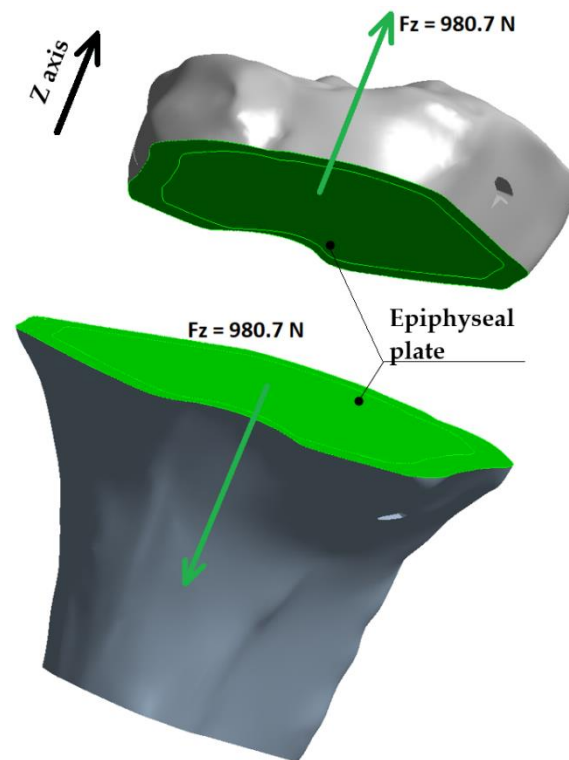
**Figure 10.** Force boundary condition—forces Fz (equivalent to 100 kg) acting on the epiphyseal plate.
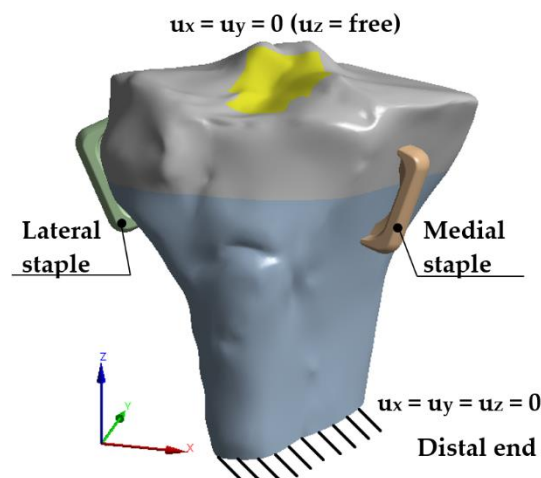


**Figure 11.** Deformation boundary conditions.

### 2.2. Experiment

The experiment was conducted to support the FEA and clinical applications, i.e., to determine the maximum loading force Fz of the bone that the staples can withstand and to partially confirm the findings of the numerical analysis. However, as the experiments are not the main goal of this article (the main goal is FEA), they were performed only once on an anatomical artificial bone [26] and once using certified bone foam blocks [27] and will be only briefly described (see Section 4: Results of the Experiment).

One of the mentioned experiments was performed on artificial bones of the SAW-BONES brand. The bones are made of composite material mimicking the properties of a real human bone, i.e., they are suitable for experimental purposes. For the use of composite bone models in experimental testing, see, e.g., [28,29].

The experiment was based on the same principles and assumptions as those used in the presented FEA. The full body of the artificial tibia was cut to obtain only the proximal part, which was subsequently split into two segments at the site of the epiphyseal plate. Both bone segments were mechanically adjusted to allow for the use of a jig. The jig consisted of a screw with a washer and nut attached to the upper bone segment (epiphysis) and of a self-tapping screw holding the lower bone segment (metaphysis-diaphysis). Staples were inserted into the bone segments (in a similar location as in FEA), bridging the epiphyseal plate. Bone segments were then pulled away from each other using the jig. Figure 12a shows a schematic drawing of the experiment. Figure 12b shows the actual experiment.
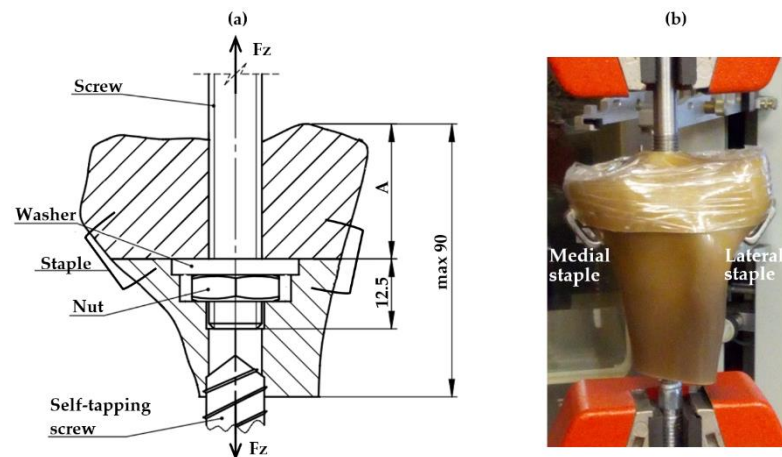


**Figure 12.** (**a**) A schematic drawing of the experiment (dimensions in mm); (**b**) Actual implementation of the experiment.

In the schematic drawing, see Figure 11a, dimension "A" details the distance of the epiphyseal plate from the top of the bone and the dimension "MAX. 90" is related to the limits of the used testing machine.

The upper bone segment in Figure 11b was wrapped in duct tape to facilitate manipulation before and during the experiment.

Used equipment:

- Model of tibia—SAWBONES, Tibia, 4th Gen., Composite, 17 PCF Solid Foam Core; see [27].
- Staples—provided by MEDIN, a.s.; see [20].
- Jig—M12 screw, M12 nut, washer (inner diameter 12 mm), ST12 self-tapping screw, all provided by MEDIN, a.s.
- Universal testing machine—TESTOMETRIC M500-50CT; see [30].

The experiment was conducted using deformation-controlled loading with a constant rate of jaw separation set to 10 mm/min.

## 3. Results of FEA

FEA was performed as described in Section 2: Materials and Methods. The distribution of equivalent stress (von Mises) in the staples was determined from the simulation of the bone growth restriction. The maximum stress occurs in the staple radius, see Figures 13 and 14.

The total displacement of staples is presented in Figure 15. In our case, the highest total displacement is at the top end of the staples and the maximum displacement is higher up in the medial staple than in the lateral one. Based on the detected deformation, we can measure the distance between the bone segments from the epiphyseal plate to obtain a rough estimation of how much the bone could grow with the staples applied. Figure 16 shows the average maximum possible growth distance between both bone segments.

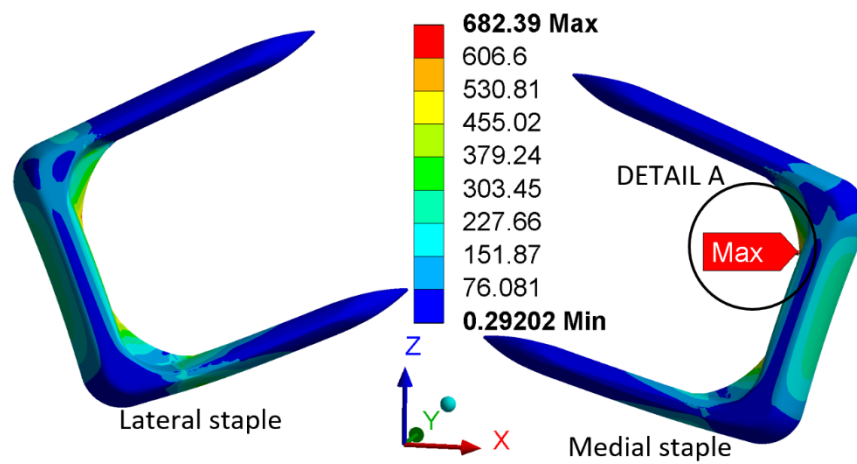The acquired FEA results are summarized in Table 3.

**Figure 13.** The distribution of the equivalent stress (von Mises) in the staples (MPa).
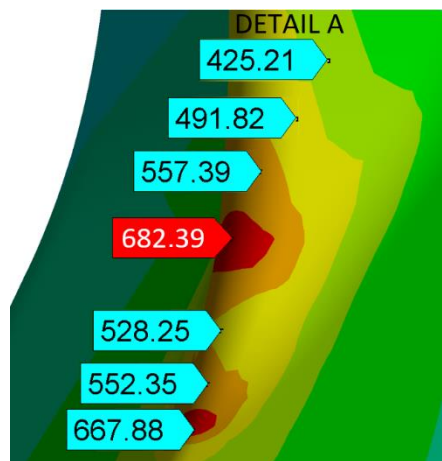


**Figure 14.** Detail "A" (see Figure 13) of the location with the maximum equivalent stress (von Mises) in the medial staple and with marked values near the maximum (MPa).
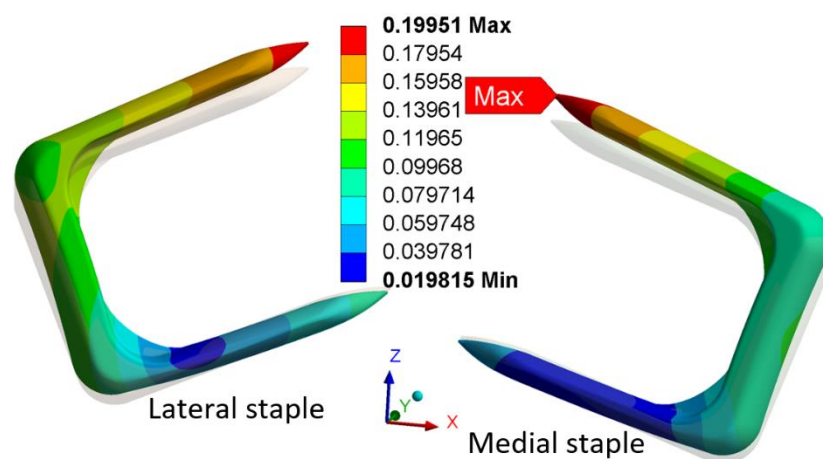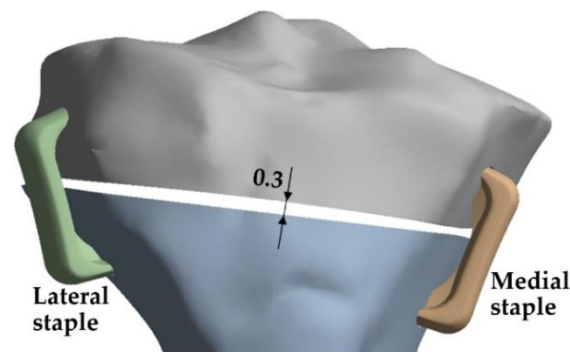


**Figure 15.** The total displacement of staples (mm), deformed + undeformed shape, deformation scale 10:1.

**Figure 16.** The average distance between the proximal and distal bone segment of the tibia (mm), deformation scale 10:1.

**Table 3.** FEA results.

|  | Value | Place |
|---|---|---|
| Maximal Equivalent von Mises Stress | 682.39 MPa | Radius of medial staple, outside of tibia; see Figures 13 and 14 |
| Maximal Displacement | 0.2 mm | Apex of medial staple, inside of tibia; see Figure 15 |
| Average distance between the proximal and distal bone segment of the tibia | 0.3 mm | Epiphysis, inside of tibia, see Figure 16 |

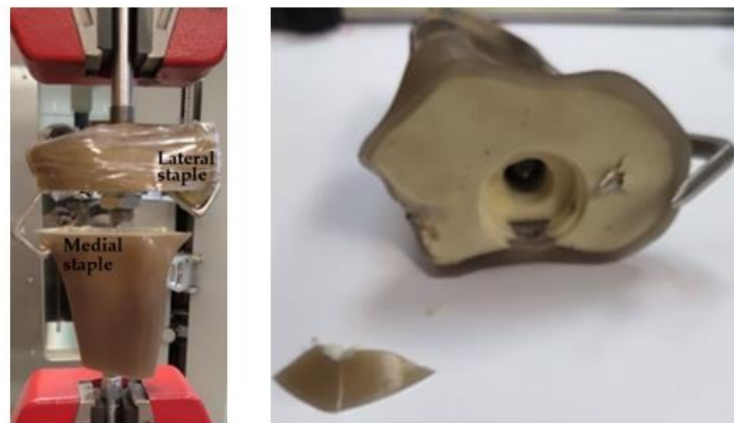## 4. Results of the Experiment

The obtained load–displacement diagram is shown in Figure 17, with the highest loading force peaking at 1612.2 N. However, during the experiment, the lower bone segment failed at the site of placement of one of the staples (lateral staple). This means that the staples are capable of withstanding even higher load than measured. The failure of the lower bone segment was also likely caused by the fragility of the artificial bone (i.e., the mechanical difference between the real and the artificial bone). The bone failure occurred at the maximum loading force.
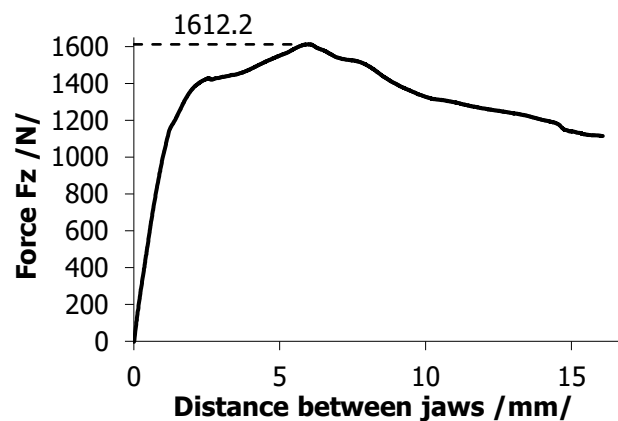


**Figure 17.** Experiment—Tensile force Fz (N) vs. separation of jaws (mm).

Figure 18 shows the artificial model bone after the experiment, along with the detail of the failure of the lower bone segment at the lateral staple site.

**Figure 18.** The model at the end of the experiment.

Apart from this experiment simulating a real-world application of Blount staples, additional experiments were performed using solid foam blocks with bone-like properties procured from SAWBONES; see [27]. The block was cut into smaller pieces to fit into our testing machine. Two pieces of the foam block were connected by a Blount staple and, as such, they were inserted into the testing machine using screws from the abovementioned jig and pulled apart. This experiment yielded similar results—the foam block always failed in the place of staple insertion, leaving the staples' structural integrity intact (similarly to the experiment on the model of the tibia); see Figure 19.
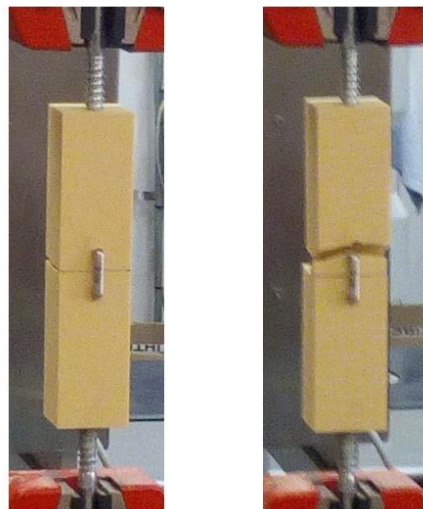


**Figure 19.** Blount staple connecting 2 blocks; left: before the experiment, right: after the experiment.

Because it was the bone blocks and not the staples that failed every time, presenting measured data for these blocks would not provide any valuable information. However, evaluation of experiments with the bone blocks (including nonlocking and locking plates, not only Blount staples) will be presented in our future work.

## 5. Discussion

A common problem regarding Blount staples observed in medical practice is not their failure (this can happen, but is very rare), but rather staple loosening or migration out of tibia [31]. To eliminate the shortcomings of staples, the tension band plate technique was invented. This technique utilizes tension band plates (i.e., two-plate, eight-plate) and screws. This newer growth arrest method eliminates problems with loosening or migration but introduces more frequent implant failure [32]. Thus, the biomechanical analysis of Blount staples can be used to better understand how the staples act under bone

growth restrictions, or, e.g., for comparison with and/or to help modify tension band plates and screws.

The numerical analysis has shown that under the chosen loading conditions of $F_z = 980.7$ N (i.e., a load equivalent to the human mass of 100 kg), the staples are safe for use. The maximum evaluated equivalent stress (von Mises) reached $\sigma_e = 682.39$ MPa. This stress does not exceed the yield strength. During the analysis, no noticeable migration of the staples from the bone was observed, which, however, can happen in real-world applications. A probable reason for this may lie in the precise placement of the staples in the bone segments under laboratory conditions, which is typically not achievable in real life, where the staples are simply hammered into the bone. The average distance between the proximal and distal bone segments of the tibia (i.e., the maximum possible change of the epiphyseal plate thickness), which is approximately 0.3 mm, is another interesting result as it tells us how much the bone can grow after epiphysiodesis (the loading in the epiphyseal plate causes slight deformations of the bone segments so the real growth could be even smaller). This possible growth is negligible, making the procedure successful from the perspective of bone growth arrest, which correlates with our initial analysis in [4], where a simpler bone material model was used.

The results presented in this paper are valid only for the particular configuration of the bone and staples and for the abovementioned material models. Other configurations using similar staples will likely yield different results, possibly moving from the elastic stress state to the elastoplastic one; this is, however, still likely to remain far from reaching the ultimate strength, making it still safe to use.

The experiment was performed in accordance with the numerical analysis to facilitate the comparison. However, during the experiment, one of the bone segments failed at the site of the bone staple insertion, and after that, only one staple held the two parts of the bone in place. This means that the obtained results are obscured and without the failure, the maximum withstandable force would be higher. Yet, the measured maximum force of $F_z = 1612.2$ N greatly exceeded our assumption of the loading (growing) force (980.7 N). In the relevant section of Figure 17, the force $F_z$ corresponds to our FEA results very well. In other experiments using certified bone foam blocks, a similar result was observed; the foam block failed, leaving the staple intact.

Unlike the numerical analysis, the experiment was burdened by real conditions introduced by the artificial bone disruption by the staples, i.e., by the bone failure at the site of staple insertion, meaning that the experiment did not fully validate the numerical model. Nevertheless, as this occurred at loading far exceeding the expected real-life loading (growing) force, both FEA and the experiment confirmed the safety of the use of staples. Still, a more ductile material (e.g., wood; see our work [33,34]) might be used instead of the model bone to avoid bone failure in future experiments. Such obtained results would probably be negligibly different from using bone.

Concerning FEA, the epiphyseal plate was modeled by virtually cutting the bone into two parts, and growth was simulated by loading the bone in this plane. For a more realistic approach, the epiphyseal plate could be modeled as a 3D object bridging the epiphysis and metaphysis-diaphysis (see Figure 6), and the growth could be simulated by prescribing displacements to relevant nodes, which is still a simplification of reality, or a more complex mathematical model could be used to consider, e.g., rate of growth, as is presented in [17]. Nevertheless, this method would not be simply verifiable by an experimental approach as we cannot easily simulate the real growth. The growth simulation remains a challenge for future scientific research.

Muscles and other soft tissues were omitted in our analysis. They might be helpful in keeping the staples from migrating from bone; however, the staple migration was not observed during our bone growth simulations. The soft tissues' effect on growth of bone is considered negligible. For similar biomechanical analyses performed without soft tissues, see, e.g., [17,23].

The paper relates to more detailed research on surgical implants, see [35–38], and on loading of the human body [39,40].

## 6. Conclusions

Results obtained by FEA and the experiment are in accordance with years of surgical experience with Blount staples.

The results show and concur that the Blount bone staples of our, or similar, designs are safe to use for clinical applications as a fracture of the staple is highly unlikely to occur.

There is a lack of information about the numerical and experimental analysis of Blount staples. Therefore, our original work fills the gap in this branch of biomechanics.

*Future Development*

For future studies, more extensive experiments could be performed measuring not only the tensile force, but also the stress inside the staples.

This paper analyzed only one type of bone staples; in the future, the focus could change to different types of staples or to pediatric plates, which eliminates the problem of staple migration.

## References

1. Fillingham, Y.A.; Kogan, M. Chapter 21—Epiphysiodesis for Limb Length Discrepancy and Angular Deformity. In *Book Case Competencies in Orthopaedic Surgery*; Frank, R.M., Forsythe, B., Provencher, M.T., Eds.; Elsevier Inc.: Amsterdam, The Netherlands, 2017; pp. 195–207. ISBN 978-0-323-39038-5. [CrossRef]
2. Eastwood, D.M.; Sanghrajka, A.P. Guided Growth: Recent Advances in a Deep-Rooted Concept. *J. Bone Jt. Surg. Br.* **2011**, *93*, 12–18. [CrossRef] [PubMed]
3. Sabharwal, S. Blount Disease: An Update. *Orthop. Clin. N. Am.* **2014**, *46*. [CrossRef]
4. Halo, T.; Frydrýšek, K.; Čepica, D.; Skoupý, O.; Michal, P.; Kraus, Š.; Havlas, V.; Kohut, J. *Numerical Simulation of Staples for Epiphysiodesis*; Vladimír, F., Ed.; Brno University of Technology Institute of Solid Mechanics, Mechatronics and Biomechanics: Brno, Czech Republic, 2020; pp. 186–189. ISSN 1805-8256. [CrossRef]
5. Métaizeau, J.P.; Wong-Chung, J.; Bertrand, H.; Pasquier, P. Percutaneous epiphysiodesis using transphyseal screws (PETS). *J. Pediatr. Orthop.* **1998**, *18*, 363–369. [CrossRef] [PubMed]

6.  Blount, W.P.; Clarke, G.R. Control of Bone Growth by epiphyseal Stapling; A Preliminary Report. *J. Bone Jt. Surg. Am.* **1949**, *31A-3*, 64–478.

7.  Shaibi, S.; Sbihi, Y.; Sdoudi, A.; Choukri, M.A.; Andaloussi, Y.E.; Fadili, M. Pseudarthrosis of Distal Radial Growth Plate Treated with Blount Clip: A Case Report. *Int. J. Surg. Case Rep.* **2021**, *87*, 106339. [CrossRef]

8.  Phemister, D.B. Operative Arrest of Longitudinal Growth of Bones in The Treatment of Deformities. *J. Bone Jt. Surg. Am.* **1933**, *15*, 1–15.

9.  Stevens, P.M. Guided Growth for Angular Correction: A Preliminary Series Using A Tension Band Plate. *J. Pediatr. Orthop.* **2007**, *27*, 253–259. [CrossRef]

10. Sabharwal, S.; Green, S.; McCarthy, J.; Hamdy, R.C. What's New in Limb Lengthening and Deformity Correction. *J. Bone Jt. Surg. Am.* **2011**, *93*, 213–221. [CrossRef]

11. Courvoisier, A.; Eid, A.; Merloz, P. Epiphyseal Stapling of the Proximal Tibia for Idiopathic Genu Valgum. *J. Child Orthop.* **2009**, *3*, 217–221. [CrossRef]

12. Jochymek, J.; Turek, J.; Peterková, T.; Urbášek, K. *Eight—Figure Plate System for Correction of Angular Deformities of Lower Limbs in Children. Initial Results*; Pohybové ústrojí: Ortotika, Praha, 2016; Volume 23, pp. 82–93.

13. Hub, J. A Study on Topology Optimization of Airplane Air Brake Bracing Beam. In *International Conference on Military Technologies (ICMT) 2019*; Institute of Electrical and Electronics Engineers Inc.: Brno, Czech Republic, 2019; p. 8870028. ISBN 978-172814593-8. [CrossRef]

14. Yang, J.C.-S.; Lin, K.-Y.; Lin, H.-H.; Lee, O.K. Biomechanical evaluation of high tibial osteotomy plate with internal support block using finite element analysis. *PLoS ONE* **2021**, *16*, e0247412. [CrossRef] [PubMed]

15. Cofaru, N.F.; Roman, M.D.; Cofaru, I.I.; Oleksik, V.S.; Fleaca, S.R. Medial Opening Wedge High Tibial Osteotomy in Knee Osteoarthritis—A Biomechanical Approach. *Appl. Sci.* **2020**, *10*, 8972. [CrossRef]

16. Joshi, J.; Manral, A.R.; Maurya, S.; Vishnoi, M. Biomechanical analysis of human tibia bone based on FEA. *Mater. Today Proc.* **2021**, *44*, 1711–1717. [CrossRef]

17. Alonso, M.G.; Bertolino, G.; Yawny, A. Mechanobiological Based Long Bone Growth Model for the Design of Limb Deformities Correction Devices. *J. Biomech.* **2020**, *109*, 109905. [CrossRef]

18. Rozehnal, D.; Hub, J.; Konvalinova, B. Innovative Processes in Preparing Models and Measuring them in the Wind Tunnel. In Proceedings of the 2021 8th International Conference on Military Technologies, ICMT 2021, Brno, Czech Republic, 8–11 June 2021; Institute of Electrical and Electronics Engineers Inc.: Brno, Czech Republic, 2021; pp. 1–6, ISBN 978-1-6654-3724-0. [CrossRef]

19. Hub, J.; Komenda, J.; Vitek, R.; Jedlicka, L. Combined Effect of Pistol Ammunition. In *International Conference on Military Technologies (ICMT), 2017*; Institute of Electrical and Electronics Engineers Inc.: Piscataway, NJ, USA, 2017; pp. 54–60. ISBN 978-153861988-9. [CrossRef]

20. MEDIN, a.s. Instruments and Implants for Traumatology [catalog]. 2018, pp. B.2.1–B.2.2. Available online: https://www.medin.cz/media/cache/file/ce/medin-traumatology-catalogue-2018-10-CS-EN_LQ.pdf (accessed on 20 August 2021).

21. *Ansys Workbench 2020*, Version R2, Software. 2020. Available online: https://aopds.com/ansys-2020-r2/(accessed on 20 August 2021).

22. Rezwan, K.; Chen, Q.Z.; Blaker, J.J.; Boccaccini, A.R. Biodegradable and bioactive porous polymer/inorganic composite scaffolds for bone tissue engineering. *Biomaterials* **2006**, *27*, 3413–3431. [CrossRef]

23. Ding, J.; Wang, F.; Jin, F.; Wu, Z.; Shen, P. Finite Element and Biomechanical Analysis of Risk Factors for Implant Failure during Tension Band Plating. *J. Int. Med. Res.* **2020**, *48*, 0300060520972075. [CrossRef] [PubMed]

24. Bylski-Austrow, D.I.; Wall, E.J.; Rupert, M.P.; Roy, D.R.; Crawford, A.H. Growth Plate Forces in the Adolescent Human Knee: A Radiographic and Mechanical Study of Epiphyseal Staples. *J. Pediatric Orthop.* **2001**, *21*, 817–823. [CrossRef]

25. Ben Achour, A.; Petto, C.; Meißner, H.; Mostofa, A.; Teicher, U.; Ihlenfeldt, S.; Lauer, G. Evaluation of a Method to Measure the Friction Coefficient between Vital Mandibular Bone and Biomedical Materials. *Biotribology* **2021**, *28*, 100198. [CrossRef]

26. "Tibia, 4th Gen., Composite, 17 PCF Solid Foam Core, Medium." SAWBONES. Available online: https://www.sawbones.com/tibia-medium-left-4th-generation-composite-3401.html (accessed on 12 June 2021).

27. "Block, Solid Foam, 10 PCF Laminated with 3 mm Solid Foam 40 PCF. SAWBONES. Available online: https://www.sawbones.com/block-10-solid-foam-1522-01-laminated-w-3mm-40-solid-foam-1522-07-finished-size-170-x-120-x-43mm-thick1522-107.html (accessed on 12 June 2021).

28. Lucas, J.F.; Chip Routt, M.L., Jr.; Eastman, J.G. Biomechanical Analysis of Retrograde Superior Ramus Screw Fixation Constructs. *J. Orthop. Trauma.* **2021**, *35*, 187–191. [CrossRef] [PubMed]

29. Murath, S.K.; Uzun, B.; Qelik, S. Comparison of five percutaneous pinning methods for unstable extra-articular distal radius fractures: A mechanical study using sawbones. *Jt. Dis. Relat. Surg.* **2021**, *32*, 51–58. [CrossRef]

30. "50 kN Machines." Testometric. Available online: https://www.testometric.co.uk/50kn/ (accessed on 5 July 2021).

31. Raab, P.; Wild, A.; Seller, K.; Krauspe, R. Correction of Length Discrepancies and Angular Deformities of the Leg by Blount's Epiphyseal Stapling. *Eur. J. Pediatr.* **2001**, *160*, 668–674. [CrossRef]

32. Schroerlucke, S.; Bertrand, S.; Clapp, J.; Bundy, J.; Gregg, F.O. Failure of Orthofix Eight-Plate for the Treatment of Blount Disease. *J. Pediatric Orthop.* **2009**, *29*, 57–60. [CrossRef]

33. Frydrýšek, K.; Michenková, Š.; Pleva, L.; Koutecký, J.; Fries, J.; Peterek Dědková, K.; Madeja, R.; Trefil, A.; Krpec, P.; Halo, T.; et al. Mechanics of Screw Joints Solved as Beams Placed in a Tangential Elastic Foundation. *Appl. Sci.* **2021**, *11*, 5616. [CrossRef]

34. Theisz, G.; Frydrýšek, K.; Fojtík, F. Medial Plate for Treatment of Distal Tibia Fractures. In Proceedings of the EAN 2015—53rd Conference on Experimental Stress Analysis, Cesky Krumlov, Czech Republic, 1–4 June 2015; Padevet, P., Bittnar, P., Eds.; CTU in Prague: Český Krumlov, Czech Republic; pp. 431–437, ISBN 978-800105735-6.

35. Pothong, W.; Phinyo, P.; Sirirungruangsarn, Y.; Nabudda, K.; Wongba, N.; Sarntipiphat, C.; Pruksakorn, D. Biomechanical Analysis of Sagittal Plane Pin Placement Configurations for Pediatric Supracondylar Humerus Fractures. *Appl. Sci.* **2021**, *11*, 3447. [CrossRef]

36. Kwon, J.; Ha, M.H.; Lee, M.G. Alternative Pedicle Screw Design via Biomechanical Evaluation. *Appl. Sci.* **2020**, *10*, 4746. [CrossRef]

37. Čada, R.; Frydrýšek, K.; Sejda, F.; Demel, J.; Pleva, L. Analysis of locking self-taping bone screws for angularly stable plates. *J. Med. Biol. Eng.* **2017**, *37*, 612–625. [CrossRef] [PubMed]

38. Frydrýšek, K.; Šír, M.; Pleva, L. Strength Analyses of Screws for Femoral Neck Fractures. *J. Med. Biol. Eng.* **2018**, *38*, 816–834. [CrossRef] [PubMed]

39. Frydrýšek, K.; Čepica, D.; Halo, T. Biomechanics—Probabilistic Anthropometry Approach for Sitting Human and Seat. In Proceedings of the 57th International Scientific Conference on Experimental Stress Analysis (EAN 2019), Luhacovice, Czech Republic, 13–16 May 2019; pp. 90–96, ISBN 978-80-214-5766-9.

40. Tai, W.-H.; Peng, H.-T.; Song, C.-Y.; Lin, J.-Z.; Yu, H.-B.; Wang, L.-I. Dynamic Characteristics of Approach Spike Jump Tasks in Male Volleyball Players. *Appl. Sci.* **2021**, *11*, 2710. [CrossRef]